Heliyon 10 (2024) e30023

Contents lists available at ScienceDirect

Heliyon

journal homepage: www.cell.com/heliyon

Research article

Radiographic chest wall abnormalities in primary spontaneous pneumothorax identified by artificial intelligence

Ming-Chuan Chiu [a], Stella Chin-Shaw Tsai [b,c], Zhe-Rui Bai [a], Abraham Lin [d], Chi-Chang Chang [e], Guo-Zhi Wang [f], Frank Cheau-Feng Lin [f,g,*]

[a] Department of Industrial Engineering and Industrial Management, National Tsing Hua University, Hsinchu, 300044, Taiwan
[b] Superintendent Office, Tungs' Taichung MetroHarbor Hospital, Taichung, Taiwan
[c] Department of Post-Baccalaureate Medicine, National Chung Hsing University, Taichung, Taiwan
[d] Engineering Management, Cornell University, Ithaca, NY, USA
[e] Department of Medical Informatics, Chung Shan Medical University Hospital, Taichung, Taiwan
[f] Department of Thoracic Surgery, Chung Shan Medical University Hospital, Taichung, Taiwan
[g] School of Medicine, Chung Shan Medical University, Taichung, Taiwan

ARTICLE INFO

Keywords:
Artificial intelligence
Chest wall
Convolutional neural network
Heatmap
Primary spontaneous pneumothorax
Scale-invariant feature transform

ABSTRACT

Primary spontaneous pneumothorax (PSP) primarily affects slim and tall young males. Exploring the etiological link between chest wall structural characteristics and PSP is crucial for advancing treatment methods. In this case-control study, chest computed tomography (CT) images from patients undergoing thoracic surgery, with or without PSP, were analyzed using Artificial Intelligence. Convolutional Neural Network (CNN) model of EfficientNetB3 and InceptionV3 were used with transfer learning on the Imagenet to compare the images of both groups. A heatmap was created on the chest CT scans to enhance interoperability, and the scale-invariant feature transform (SIFT) was adopted to further compare the image level. A total of 2,312 CT images of 26 non-PSP patients and 1,122 CT images of 26 PSP patients were selected. Chest-wall apex pit (CAP) was found in 25 PSP and three non-PSP patients ($p < 0.001$). The CNN achieved a testing accuracy of 93.47 % in distinguishing PSP from non-PSP based on chest wall features by identifying the existence of CAP. Heatmap analysis demonstrated CNN's precision in targeting the upper chest wall, accurately identifying CAP without undue influence from similar structures, or inappropriately expanding or minimizing the test area. SIFT results indicated a 10.55 % higher mean similarity within the groups compared to between PSP and non-PSP ($p < 0.001$). In conclusion, distinctive radiographic chest wall configurations were observed in PSP patients, with CAP potentially serving as an etiological factor linked to PSP. This study accentuates the potential of AI-assisted analysis in refining diagnostic approaches and treatment strategies for PSP.

1. Introduction

Commonly afflicting young men between the age of 15–25 years, primary spontaneous pneumothorax (PSP) occurs with an incidence rate as high as 7.4–18 per million men [1]. In many instances, small pneumothorax may resolve on their own, and individuals may not require extensive medical intervention [2]. However, the severity of PSP can vary, and larger pneumothorax may

* Corresponding author. 110, Section 1, Jian-Guo North Road, Taichung, 40201, Taiwan.
E-mail address: tpn@csmu.edu.tw (F.C.-F. Lin).

https://doi.org/10.1016/j.heliyon.2024.e30023
Received 7 June 2023; Received in revised form 18 April 2024; Accepted 18 April 2024
Available online 30 April 2024

Abbreviations

AI	artificial intelligence
BB	Bleb and bullae
CNN	Convolutional Neural Network
CAFAP	Chest-wall apex fat pad
CAP	Chest-wall apex pit
ELC	emphysematous-like change
PSP	Primary spontaneous pneumothorax
SIFT	Scale-invariant feature transform
VPD	vascular penetration defect

cause more significant respiratory distress. Rarely, a tension pneumothorax, where air accumulates and progressively compresses the lung and mediastinum, can lead to life-threatening complications [3,4]. Pneumothorax may be spontaneous, traumatic, or iatrogenic in nature. Spontaneous pneumothorax occurs without an outside force, and PSP occurs without any underlying diseases [5,6].

With the advances in surgical optical resolution and instrumentation, all the ruptured lung cases in PSP can be identified at the apical area of the chest cavity, including the apex of the upper lobe and the superior segment of the lower lobe of the lung [7]. In a previous study, chest wall deformity was found to be linked to PSP [8]. In addition, our previous report on the association of vascular penetration defects (VPD) and PSP was among the first in medical literature to describe the etiological relationship between chest-wall structural defects and PSP [9]. Nevertheless, only nine of 22 patients in the study had VPD, indicating that VPD could not explain most of the PSP incidence. It was further confirmed in a recent study where similar structural defects were present in 45 of 297 patients (15.2 %) [10]. In recent clinical observations, the presence of a chest-wall apex pit (CAP) has been identified as a noteworthy phenomenon replacing VPD. In this study, our primary objective is to investigate and establish a potential etiological link between specific chest wall structural characteristics, particularly CAP, and the occurrence of PSP.

Current advances in artificial intelligence (AI) and deep learning have enabled computer algorithms to detect subtle patterns in medical imaging that may escape human recognition. The cutting-edge development of deep learning technology has helped alert clinicians when abnormalities are detected on chest radiographs [11–13]. Briefly, gradient-based learning was applied to the image reorganization to extract features from images, which proceeded to the next volume base for further feature extraction [14]. Accordingly, the learning efficiency of the neural network was enhanced compared to traditional image recognition. General applications of neural networks possess a higher learning efficiency and can potentially become the foundation of several AI models in the future. In particular, convolutional neural networks (CNNs) can be trained to identify visual features associated with specific diseases or outcomes using large labeled datasets; it has been used to detect pulmonary nodules [15].

Utilizing these AI methodologies for the examination of chest CT scans has the potential to unveil previously unrecognized radiographic indications associated with the onset of PSP. This is particularly crucial as such anomalies are challenging for medical professionals to quantify without a standardized model for distinguishing abnormalities in the chest wall. Determining structural factors associated with PSP holds great clinical significance, as this could point to new strategies for treatment and prevention in susceptible individuals. This study employs AI-powered image recognition to uncover potential chest wall abnormalities that may represent an important etiological discovery in PSP.

2. Study design and methods

2.1. Study design

In this retrospective study, participants were categorized into two groups: the PSP group and the non-PSP group. The PSP group consisted of patients who underwent thoracic surgery at a medical center in central Taiwan during the years 2020 and 2021. The non-PSP group comprised individuals who received thoracic surgery in the year 2021 and were specifically selected for their younger age to as closely match the age range of the PSP group as possible. The subject and control were matched 1:1 with age. Inclusion criteria encompassed patients from both groups who underwent thoracic surgery within the designated timeframe and possessed preoperative chest CT images. Exclusion criteria were applied to exclude patients with secondary spontaneous pneumothorax resulting from underlying lung disease, traumatic or iatrogenic pneumothorax, a history of prior thoracic surgery, and instances where imaging artifacts or poor image quality precluded rigorous analysis. The diagnostic criteria for PSP involved clinical presentation and radiographic evidence of pneumothorax without an identifiable cause. The control group, consisting of non-PSP patients, underwent thoracic surgery for reasons such as lung cancer resection. The most recent preoperative CT images for each patient were scrutinized, with those displaying significant motion artifacts or inadequate image quality being excluded from the analytical process.

2.2. Chest-wall apex pit

All the blebs that occurred in structural defects were named the chest-wall apex pit (CAP, Fig. 1A–C). CAP was defined as a convex area surrounded by the first or second rib and mainly by the subclavian artery. Structurally, the apex of the chest wall was smoothly

rounded in shape in individuals without PSP but was irregular with inward sharp angle pits at the apex among PSP patients. The computed tomography (CT) of the patients with and without PSP was reviewed by a thoracic surgeon. The demography and the CAP were collected. CAP identification was performed through a round of CT image review by two thoracic surgeons blinded to any clinical information.

2.3. Convolutional neural network (CNN)

This study used the CNN-based binary classification models to identify CAP. The establishment of the model was divided into two stages: data preprocessing and CNN model training, as shown in eAppendix.

Data preprocessing was performed as illustrated (eFig. 1). Multiple images per patient were used, leading to a larger overall sample size for model development. Patients were selected for training, validation, and testing randomly. The testing was done before and after the data augmentation. "Data Filtering" coronal views were selected as ten approximately 5 mm images around the level of the aorta, capturing complete chest wall contours. Air was erased from the images; only the chest wall and great vessels were retained. We also performed data augmentation techniques, including rotation, flipping, noise addition, and brightness variation, to increase the size of the dataset and make the model more robust [16,17].

Preprocessed chest CT images underwent CNN model training, validation, and testing. In this study, EfficientNetB3(Google, Mountain View, California) [18] and InceptionV3(Intel Corporation, Santa Clara, California) [19] were used for feature identification of PSP and, through transfer learning, the model parameters were trained on the ImageNet [20] (Stanford Vision Lab, Stanford, CA) dataset and were used as the initial parameters of the models.

EfficientNetB3 architecture was a new benchmark network proposed by Google. The model applied a new network scaling method that uniformly scaled the network depth (number of network layers), width (number of channels), and image resolution (input image size) using compound coefficients to scale within a fixed resource limit and achieve higher accuracy. The network architecture diagram can be found at Towards Data Science [21].

The network architecture of InceptionV3 can be found at Intel [22]. The most significant improvement in its model architecture was factorization, which decomposed the 7×7 and 3×3 convolutions into four (two each) one-dimensional convolution series (1×7 and 7×1) and (1×3 and 3×1), respectively. This not only speeds up the calculation but also further increases the nonlinearity of the

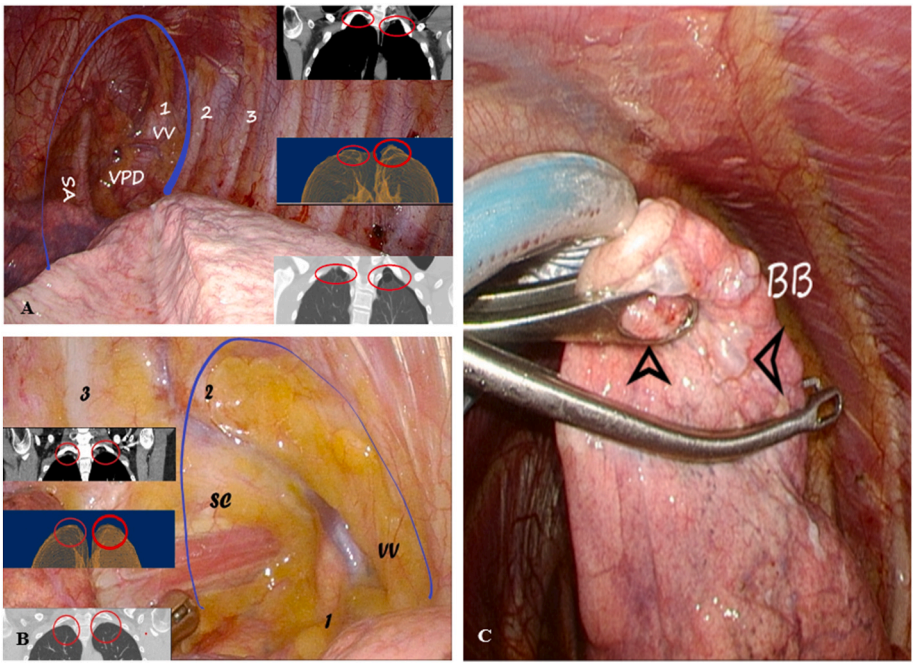

Fig. 1. The formation of the bleb in the chest wall apex pit.
A. The chest wall of a PSP patient. The prominent subclavian artery and 1st rib encircled a convex area at the apex of the chest wall. The corresponding CT scan on the right upper side showed the same pit. The chest-wall apex pit (CAP) was encircled. The right middle picture is a 3D lung image showing an abnormal extra-growth project from the smooth round normal part of the lung which herniated into the CAP, modeling the correspondent chest wall on the right upper coronal CT. The insert at the lower right confirms that the blebs fit into the CAP.
B. The chest wall apex of a 165 cm 67 kg male. The area circled by the 1st and 2nd rib was cushioned with chest-wall apex fat pad (CAFAP). The subclavian vessels and rib hid in the fat. The chest wall surface was smooth.
C. A resected ELC lung was found with bleb. The lung above the clamp was fragile, whereas below the clamp showed an ELC. BB denotes the original bleb. Arrowhead, the bleb just generated due to the grasp of the ring clamp, where one bleb was produced in the ring. CAP, chest wall apex pit; SA, subclavian artery; SC, sympathetic chain; VPD, Vascular penetration defect; VV, Vertebral Vein.

network.

Transfer learning is a machine learning method that transfers knowledge from one domain (source domain) to another (target domain) so that the target domain can achieve better learning effects [22,23]. The CNN network structure found in the preliminary selection of this study has been pre-trained in the ImageNet image data set, thus greatly improving the training efficiency of this study [20].

2.4. Valuation indicators of measurement of classification performance

The true and false positive and negative rates were calculated, respectively. The indicators of performance measurement in CNN classification included accuracy, precision (positive prediction value), recall (sensitivity), and F1-score (1 = perfect). These indicators are used to measure the performance of the model in identifying CAP accurately [24].

2.5. Interpretability validations

2.5.1. Heatmap

To further verify whether the model can accurately capture the lesion features of the data, this study extracted the CNN attention features and used the heat map visualization method [17].

2.5.2. Chest wall similarity comparison by the scale-invariant feature transform

The feature point extraction method, scale-invariant feature transform (SIFT), is an algorithm for detecting local features [25–27]. Dr. Lowe proposed this method to identify extreme values in the spatial scale point and to find out the position, scale, and orientation information of the extreme point [28]. In the field of image recognition, local features can be used to help identify objects through description and detection. The features extracted by SIFT were so prominent that accurate detection results could be achieved even in variable angles of view, distances, rotations, and color temperatures, which can subsequently be applied to robot map perception and navigation, impact stitching, 3D model building, gesture recognition, and image tracking.

2.6. Image preprocessing

The drawing software Labelme [29], was used to mask the lungs (air) and left chest wall specifically to avoid the feature extraction method SIFT used in the subsequent comparison methods from capturing excessive and unnecessary image features, as shown in eFig. 2A. Each datum was pre-processed, reconstructed by LabelMe using three-dimensional images, converted into a 2-dimensional image, and underwent grayscale data preprocessing [16], as shown in eFig. 2B.

2.7. Scale-invariant feature transform of the chest wall

The scale-invariant feature transform of the chest wall was evaluated using structural similarity comparisons categorized into PSP versus non-PSP, PSP versus PSP, and non-PSP versus non-PSP. In the case of PSP versus non-PSP, the comparisons were conducted sequentially, starting with PSP 1st versus non-PSP 1st, 2nd, 3rd; followed by PSP 2nd versus non-PSP 2nd, 3rd, 4th, and so forth, resulting in a total of 30 comparisons. Similarly, for PSP versus PSP and non-PSP versus non-PSP, the comparisons involved pairs such as 1st versus 2nd, 3rd, 4th; 2nd versus 3rd, 4th, 5th, and continued up to the 30th comparison, ensuring a systematic and comprehensive analysis.

3. Results

Several demographic factors varied between the PSP and non-PSP patients. Firstly, the mean age of PSP patients was lower than that of the non-PSP group. Secondly, higher male-to-female percentage of participants was found in the PSP group, compared to the

Table 1
Demography of patients with and without primary spontaneous pneumothorax.

	PSP		non-PSP		P
	N/mean	%/SD	N/mean	%/SD	
	26		26		
Age	23.5	8.4	35.9	2.7	<0.001[a]
Gender (M/F)	21/5	80.8/19.2	13/13	50/50	0.021[a]
Height (cm)	172.3	8.3	166.8	8.1	0.019[a]
Weight (kg)	55.8	9.3	68.3	13.3	<0.001[a]
BMI	32.3	4.4	40.8	6.6	<0.001[a]
Smoking	4	15.4	2	7.7	0.385
CAP	25	92.2	3	11.5	<0.001[a]

[a] $P < 0.05$.

non-PSP group. Thirdly, the BMI indicated that PSP patients were more underweight. Additionally, surgeons verified one PSP without CAP and three non-PSP with CAP on CT. The complete patient demographic profile is shown in Table 1.

The dataset had a total of 3,434 thoracic image datasets, in which the data were divided into two categories: 26 non-PSP patients with a total of 2,312 images and 26 PSP patients with a total of 1,122 images. Data filtering operations were conducted to lay a good foundation for model training. Consequently, 237 and 218 coronal images with complete chest contours were selected from non-PSP and PSP patients, respectively. After filtering out images that did not match the criteria set by our research team, we randomly divided and assigned patients into training, validation, and testing datasets for both PSP and non-PSP (eTable 1A). We adjusted the assignment until the number of images in training, validation, and testing datasets matches 8:1:1 ratio before the augmentation process. From the 218-PSP dataset, 4 patients were randomly selected with a total of 22 and 22 images for validation and test. From the 237-non-PSP dataset, 5 patients were randomly selected with a total of 23 and 24 images. This approach avoids using same patients' data between training set, validation set, and test set while ensuring appropriate ratios across each set. The data augmentation included flat flip, Gaussian noise, filtering, brightening and darkening once each, and rotating every 24° for a total of 15 times. In addition, the non-PSP category was enhanced by 20 times to 4,740 images and PSP category was enhanced by 20 times to 4,360 images. The data augmentation is shown in eFig. 1.

eTables 1B and C showed the recorded hyperparameter combinations and orthogonal table results of EfficientNetB3 model training. In this study, five factors were selected for parameter optimization, and each factor contained four levels, resulting in a total of 1,024 experimental groups and sums. To save the experiment time and ensure that the optimal parameter results were found, the L_{16} orthogonal table was used according to the Taguchi method. As shown in eTable 1B, the unified size of the picture input was 300 × 300. The model training material included 7,280 CT images of the training data set, using the environment of Python 3.7 and Tensorflow 1.15 on Win 10, Intel Core i5-8400 2.8 GHz CPU, NVIDIA GeForce RTX 2080 Ti GPU computer, training for 50 rounds, and 164 pictures per round, which lasted approximately 4.5 h.

eTable 1A, B also demonstrate the hyperparameter combination and orthogonal table results trained by the InceptionV3 model, with uniform input image size, and the image sequence randomized and divided repeatedly according to the ratio. The model training materials included CT images of 7,372 training data sets, training for 50 epochs lasting approximately 4.5 h.

The true positive/negative and false positive/negative rates, described in Table 2, recorded the classification between PSP and non-PSP results of the CNN models after training on the test data set. Overall, the EfficientNetB3 model achieved an accuracy of 93.47 % and an F1-score of 93.32 % on the 46-test set. In light of the small size of the test set, a Receiver Operating Characteristic (ROC) curve was employed to investigate the impact of this size limitation. With an ROC curve area of 0.936 and a significance level of $p < 0.001$, it can be concluded that the model has successfully developed a dependable PSP classification system. After augmentation, the EfficientNetB3 model achieved an accuracy of 95.60 % and an F1-score of 95.84 % on the 903 CT coronal imaged tested exceeding the performance of InceptionV3.

The heatmap revealed that the CNN model specifically targeted the upper part of the chest wall while distinguishing the PSP/non-PSP, further suggesting that the CNN model could effectively capture the lesion features and their location correlation (Fig. 2).

An example of a similarity comparison between PSP and non-PSP is demonstrated in eFig. 3. The comparison results of the two groups, such as the average similarity between PSP and non-PSP images, are shown in Table 3. The mean similarity of the within-group comparison was almost 60 %, which was higher than those of the between-group comparison with approximately 50 % similarity; the mean similarity for the within-group was about 10.55 % higher than that of the between-groups, with $p < 0.001$ in student's independent t-tests.

4. Discussion

This is the first study to demonstrate the marked structural difference in the chest wall of patients with and without PSP. The CAP was found in all except one of PSP, in contrast to three of 26 non-PSP, patients. The EfficientNetB3 CNN correctly depicted the difference in the chest wall structure between PSP and non-PSP patients with an accuracy of 93.47 %. The heatmap showed that the differences in the CNN workings were in the apex area. The SIFT further confirmed the structural differences in the visible image level, where the images were similar within each group with or without PSP and were different between the PSP and non-PSP groups. This observation was more prominent in the lung apex, and the findings provide solid evidence of the distinct chest wall structures of PSP, as identified by CAP.

The etiology of PSP remains unclear. Based on previous studies, three factors were considered possible causes of PSP, i.e.,

Table 2
Testing results of PSP classification performance by CNN models.

Model	TP	TN	FP	FN	Accuracy	Precision	Recall	F1-score
EfficientNetB3 Non-augmented	21	22	2	1	0.9347	0.9130	0.9545	0.9332
EfficientNetB3 Augmented	426	444	11	26	0.9560	0.9748	0.9425	0.9584
InceptionV3 Augmented	414	427	28	41	0.9242	0.9367	0.9099	0.9231

TP, TN, FP, FN: true positive, true negative, false positive, false negative. Precision = specificity. Recall = sensitivity.

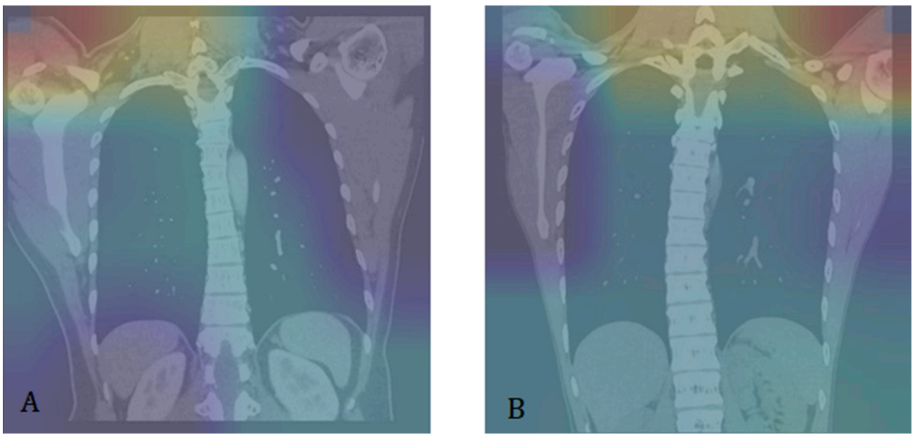

Fig. 2. The heatmap of non-PSP and PSP. B. The CNN working area was concentrated at the apex of the chest wall. A and B represent images from two different patients.

Table 3
Comparison of similarities of SIFT.

	mean	SD	P	
PSP vs. non-PSP	48.6	5.1	<0.001[a]	<0.001*
PSP vs. PSP	59.2	2.6	0.900	
non-PSP vs. non-PSP	59.1	2.7		

[a] $P < 0.05$, unit: percentage.

inflammation, emphysematous-like change (ELC), and bleb/bullae (BB) formation. Hypoxia, inflammation, and apoptosis were found in the PSP resected tissue with macrophages, lymphocytes, interleukins, tumor necrotic factors, and post-inflammatory fibrosis [6,30]. Accordingly, the overexpression of matrix metalloproteinases could only partially explain the occurrence of PSP [31]. Therefore, in patients with PSP, an inflammatory change with mesothelial cell disruption was observed, potentially creating an ELC and developing BBs; however, the cause of inflammation has not yet been established.

BBs were found to have a high correlation with PSP incidence [5–7,32]. BBs predicted recurrent pneumothorax with a positive predictive value of 68.1 %, a negative predictive value of 93.9 % for ipsilateral, a positive predictive value of 19 %, and a negative predictive value of 100 % for contralateral [33]. Blebs (Reid type 1 bulla) are defined as air in the visceral pleura separating the lamina elastica externa and interna and are the most frequently found among non-smoker PSP patients [34]. The mesothelial cells were disrupted and replaced by inflammatory and fibrotic cells.

One of the major findings of surgery and pathology in PSP is the ELC at the apex of the lung, which can explain some of the cases where no bleb was noted [5–7,35]. Smoking is the primary etiology of emphysema, but for non-smoking PSP patients, the etiology is indeterminate. Under pathological examination, emphysematous changes occur around the BB. A previous study revealed that blind resection of the apex area without BB did not prevent further recurrence [36]. An air leak site occurs without often being observed during surgery. Noppen et al. examined the air leak area and found that not all were located at BBs [37–39]. In some cases, the inflammatory reaction disrupted the mesothelium without forming the bleb with a pore diameter of 10–20 μm in the visceral pleura [5,6,39]. A staple line recurrent BB was noted in 16 of 30 recurrent post-operative PSPs [40], possibly indicating the weakness and traumatic nature of the staple line on the ELC area that could trigger a new BB formation.

PSP occurs commonly among tall and lightweight males [35], especially in those with a height increase that was ahead of the body weight at the age of 11–14 years, with taller, narrower, and flatter thoraces [41]. The difference in the body configuration growth might have created a structural difference at the apex of the thoracic cage and affected the CAP. Because of low BMI, the chest-wall apex fat pad (CAFAP) was minimal in these patients and the ribs and vessels were protruded in the pleural cavity, where abnormalities frequently occurred (eFig. 4). On the other hand, females of the same age have, on average, more fat than their male counterparts, which may explain the gender difference in the incidence of PSP. As age increases, the BMI and the fat, including CAFAP, increase, providing a plausible explanation for the decreased CAP and incidence of PSP among older individuals. Furthermore, the VPD is also concentrated in the CAP and absent in other areas; hence, the vessel penetrates the chest wall in the absence of a CAFAP cushion, precipitating a hole. The relationship of chest wall deformities and pneumothorax has been previously established [8,42,43]. Contrary to previous assumptions, this study proposes that VPD may not be the primary cause of PSP; rather, CAP emerges as a potential culprit. The strong correlation observed between VPD and PSP may be attributed to a shared factor—the absence of the CAFAP cushion. This

perspective offers a nuanced understanding, suggesting that CAP, rather than VPD, may play a pivotal role in the development of PSP, with the association to VPD arising from a common root cause, the deficiency of the CAFAP cushion. BB were observed in 26.5 % of cases with an elevated Haller index in individuals with pectus excavatum, demonstrating a bleb formation odds ratio of 2.221 (95 % confidence interval 1.481–3.330, $p < 0.001$) [8].

The apex of the lung sustains the most negative pressure, with an associated expanded alveolar space, where ELC and BB occur [44]. This may explain the anteriorly located BB among bedridden patients [45]. In cases where the chest wall is not smooth with a pit in the chest wall, upon negative pleural pressure, the lung will "balloon" to fit the CAP, which may lead to further abnormalities. As described by Yang et al. [46], the lung apex might be strangled in the CAP, and the trapped part would be desynchronized with other parts of the lung in respiratory movement. This would induce shearing forces and stretch injuries, resulting in inflammation. Stretch injury theory has not been mentioned in pneumothorax but in ARDS, as it causes physical injury and inflammation [47]. Cyclic stretching and opening/closing of the alveoli physically detach the cells from the basement membrane, leading to cell death and the potential damage of fluid circulation and induction of proinflammatory cytokines and chemokines. Consequently, compensatory emphysema may occur, which overinflates a part of the lung in response to either surgical removal or decreased size of another part of the lung. The apex of the lung herniates to CAP, and the extra space induces compensatory emphysema. The lung is protected from vigorous respiration movement against the chest wall since friction happens between the two layers of the pleura where a lubricant is present [48]. Subsequently, friction of the trapped lung to the chest wall increases due to the irregularity of the chest wall and less pleural fluid due to gravity. The prominent subclavian artery provides vibration at this fixed lung, which may cause abrasion injury to the emphysematous lung that forms blebs. Furthermore, the strong negative pressure of the apex and the inflammatory lung may trap air in the herniated lung, similar to that in ELC and BB. This pathogenesis explains the occurrence of inflammation, ELC, and BB among patients with PSP. The body configuration, gender difference, and reason for the association of chest wall deformity with PSP were also answered.

In our CNN model, the accuracy of the PSP prediction was 96.94 %; however, the CT from the EfficientNetB3 model may further predict the risk of PSP. This evidence may warn young people with similar chest wall structures. According to this critical finding, an ongoing novel surgical design aims to prevent the recurrence of PSP.

The relatively small sample size is a limitation of our study and confirmation in larger cohorts is warranted. Machine learning techniques can be trained better with a larger size dataset, despite the fact that these images originated from the same source. Augmentation also allows the model to perform well under different image conditions. Importantly, the model demonstrated high accuracy not just on the training data but also on the held-out test set, supporting its generalizability. The study also acknowledges the potential for confounding arising from uneven matching between the PSP and non-PSP groups. Specifically, it has been observed that male, young, tall, and thin individuals are at a higher risk of developing PSP. The non-PSP group was carefully selected based on age, with a preference for younger individuals. However, despite these efforts, there remains a notable age difference of 12.5 years between the PSP and non-PSP groups, along with variations in other traits. The limited availability of young non-PSP patients who have undergone thoracic surgery contributes to this imbalance and explains the observed skew in age distribution. Nonetheless, the mean similarity for the within-group was about 10.55 % higher than that of the between-groups, with $p < 0.001$, which further supports that the influence of biases in this study was minimal.

For future investigations, a chest wall deformity model inducing bleb and PSP should be established in animals or in a phantom to test the hypothesis directly. Additionally, the structure of the thoracic cage should be studied according to sex since 80 % of PSPs were detected in males [49], who could have proportional differences in the CAFAP. PSP is noted to be rare among those aged 30 and above. Therefore, a cohort study could follow the thoracic cage structures of PSP patients and identify structural changes to further establish visceral pleural thickening according to age.

With the use of Artificial Intelligence processes such as CNN, heatmap, and SIFT, the radiographic chest wall structure of patients with PSP was found to be different from those without, with the presence of CAP and possible VPD. These chest wall abnormalities may be an important structural etiological factor for PSP. Hence, the detection of CAP on chest CT should warrant a keen watch out for the occurrence of PSP. Furthermore, the findings of this study also point to the future development of potential treatment modalities to prevent the recurrence of PSP.

Ethics statement

The study protocols were rigorously reviewed and received ethical clearance from the Institutional Review Board (IRB) of Chung Shan Medical University Hospital (Approval No: CS2-22114). In consideration of the study's design, the IRB granted a waiver for patient informed consent.

Data availability statement

The dataset is accessible at the following link:
Lin, Frank (2024), "CAP study", Mendeley Data, V1, https://doi.org/10.17632/4wgzgpdbyr.1.

Fundings

This research received grants from the Ministry of Science and Technology, Taiwan (grant number: MOST 109-2628-E-007-002-MY3) and Tungs' Taichung MetroHarbor Hospital (grant number: TTMHH-R1120006).

CRediT authorship contribution statement

Ming-Chuan Chiu: Writing – original draft, Validation, Software, Methodology, Investigation, Funding acquisition, Formal analysis, Data curation, Conceptualization. **Stella Chin-Shaw Tsai:** Writing – review & editing, Validation, Funding acquisition, Formal analysis. **Zhe-Rui Bai:** Writing – original draft, Validation, Software, Investigation, Formal analysis, Data curation. **Abraham Lin:** Writing – review & editing, Validation, Methodology. **Chi-Chang Chang:** Writing – review & editing, Methodology, Investigation, Formal analysis, Data curation. **Guo-Zhi Wang:** Writing – review & editing, Methodology, Investigation. **Frank Cheau-Feng Lin:** Writing – review & editing, Validation, Supervision, Resources, Project administration, Methodology, Investigation, Funding acquisition, Formal analysis, Conceptualization.

Declaration of competing interest

The authors declare that they have no known competing financial interests or personal relationships that could have appeared to influence the work reported in this paper.

Acknowledgements

We would like to thank Chuck Lin for his thoughtful comments and editorial support.

Appendix A. Supplementary data

Supplementary data to this article can be found online at https://doi.org/10.1016/j.heliyon.2024.e30023.

References

[1] M. Noppen, Spontaneous pneumothorax: epidemiology, pathophysiology and cause, Eur. Respir. Rev. 19 (117) (2010) 217–219.
[2] T. Sugibayashi, et al., Deep learning for pneumothorax diagnosis: a systematic review and meta-analysis, Eur. Respir. Rev. 32 (168) (2023).
[3] Y.-W. Tung, et al., Bilateral developing reexpansion pulmonary edema treated with extracorporeal membrane oxygenation, Ann. Thorac. Surg. 89 (4) (2010) 1268–1271.
[4] Z. Liu, et al., Sudden unexpected death due to spontaneous pneumothorax caused by ruptured bilateral pulmonary bullae, J. Forensic Sci. 66 (6) (2021) 2499–2503.
[5] D. Haynes, M.H. Baumann, Pleural controversy: aetiology of pneumothorax, Respirology 16 (4) (2011) 604–610.
[6] S. Grundy, A. Bentley, J.M. Tschopp, Primary spontaneous pneumothorax: a diffuse disease of the pleura, Respiration 83 (3) (2012) 185–189.
[7] A.K. Ayed, C. Chandrasekaran, M. Sukumar, Video-assisted thoracoscopic surgery for primary spontaneous pneumothorax: clinicopathological correlation, Eur. J. Cardio. Thorac. Surg. 29 (2) (2006) 221–225.
[8] H.K. Huang, et al., Severity of pectus excavatum is a risk factor for primary spontaneous pneumothorax, World J. Surg. 44 (6) (2020) 2035–2041.
[9] F.C. Lin, et al., Vascular-penetration defect detected in parietal pleura of primary spontaneous pneumothorax, Interact. Cardiovasc. Thorac. Surg. 19 (5) (2014) 861–863.
[10] H. Shiiya, et al., Parietal pleural small holes found in patients with primary spontaneous pneumothorax associated with relatively mild chest wall flatness: a retrospective study, J. Thorac. Dis. 14 (9) (2022) 3255–3264.
[11] Y.L. Thian, et al., Effect of training data volume on performance of convolutional neural network pneumothorax classifiers, J. Digit. Imag. 35 (4) (2022) 881–892.
[12] S. Park, et al., Deep learning-based detection system for multiclass lesions on chest radiographs: comparison with observer readings, Eur. Radiol. 30 (3) (2020) 1359–1368.
[13] J.S. Ahn, et al., Association of artificial intelligence-aided chest radiograph interpretation with reader performance and efficiency, JAMA Netw. Open 5 (8) (2022) e2229289.
[14] Y. Lecun, et al., Gradient-based learning applied to document recognition, Proc. IEEE 86 (1998) 2278–2324.
[15] W. Shen, et al., Multi-scale convolutional neural networks for lung nodule classification, Inf. Process Med. Imaging 24 (2015) 588–599.
[16] F. Ciompi, et al., Towards automatic pulmonary nodule management in lung cancer screening with deep learning, Sci. Rep. 7 (1) (2017) 46479.
[17] M. Zhao, Y. Wei, K.K.L. Wong, A Generative Adversarial Network technique for high-quality super-resolution reconstruction of cardiac magnetic resonance images, Magn. Reson. Imaging 85 (2022) 153–160.
[18] M. Tan, Q. Le, 36th international conference on machine learning, ICML 2019. ICML, Long Beach, 2019.
[19] C. Szegedy, et al., Rethinking the inception architecture for computer vision, in: Proceedings of the IEEE Conference on Computer Vision and Pattern Recognition, 2016.
[20] ImageNet, ImageNet Is an Image Database Organized According to the WordNet Hierarchy (Currently Only the Nouns), in Which Each Node of the Hierarchy Is Depicted by Hundreds and Thousands of Images. The Project Has Been Instrumental in Advancing Computer Vision and Deep Learning Research. The Data Is Available for Free to Researchers for Non-commercial Use, 2021. Available from: https://www.image-net.org/. (Accessed 19 October 2022).
[21] V. Agarwal, Complete architectural details of all EfficientNet models, Data Sci. (2020) [webpage], https://towardsdatascience.com/complete-architectural-details-of-all-efficientnet-models-5fd5b736142. (Accessed 19 October 2022).
[22] Adam, Inception V3 Deep Convolutional Architecture for Classifying Acute Myeloid/Lymphoblastic Leukemia, 2019. Available from: https://www.intel.com/content/www/us/en/developer/articles/technical/inception-v3-deep-convolutional-architecture-for-classifying-acute-myeloidlymphoblastic.html. (Accessed 19 October 2022).
[23] J.J. Bird, et al., Cross-domain MLP and CNN transfer learning for biological signal processing: EEG and EMG, IEEE Access 8 (2020) 54789–54801.
[24] X. Ma, et al., Comparison and development of machine learning tools for the prediction of chronic obstructive pulmonary disease in the Chinese population, J. Transl. Med. 18 (1) (2020) 146.
[25] Y. Xu, et al., 3D-SIFT-Flow for atlas-based CT liver image segmentation, Med. Phys. 43 (5) (2016) 2229.
[26] D.H. Lee, D.W. Lee, B.S. Han, Possibility study of scale invariant feature transform (SIFT) algorithm application to spine magnetic resonance imaging, PLoS One 11 (4) (2016) e0153043.
[27] W. Cheung, G. Hamarneh, n-SIFT: n-dimensional scale invariant feature transform, IEEE Trans. Image Process. 18 (9) (2009) 2012–2021.

[28] D.G. Lowe, Distinctive image features from scale-invariant keypoints, Int. J. Comput. Vis. 60 (2) (2004) 91–110.
[29] B.C. Russell, et al., LabelMe: a database and web-based tool for image annotation, Int. J. Comput. Vis. 77 (1) (2008) 157–173.
[30] H.Y. Fang, et al., Microarray detection of gene overexpression in primary spontaneous pneumothorax, Exp. Lung Res. 36 (6) (2010) 323–330.
[31] Y.F. Huang, et al., Association of MMP-2 and MMP-9 expression with recurrences in primary spontaneous pneumothorax, Kaohsiung J. Med. Sci. 33 (1) (2017) 17–23.
[32] F.M. Schramel, P.E. Postmus, R.G. Vanderschueren, Current aspects of spontaneous pneumothorax, Eur. Respir. J. 10 (6) (1997) 1372–1379.
[33] C. Casali, et al., Role of blebs and bullae detected by high-resolution computed tomography and recurrent spontaneous pneumothorax, Ann. Thorac. Surg. 95 (1) (2013) 249–255.
[34] J.Y. Huang, et al., Human papillomavirus is associated with adenocarcinoma of lung: a population-based cohort study, Front. Med. 9 (2022) 932196.
[35] R. Hallifax, Aetiology of primary spontaneous pneumothorax, J. Clin. Med. 11 (3) (2022).
[36] M. Vayvada, Y. Tezel, Ç. Tezel, Is it a myth to perform blind apical wedge resection in primary spontaneous pneumothorax surgery to improve recurrence rates? J. Minimal Access Surg. 18 (2) (2022) 279–283.
[37] A. De Smedt, et al., Characterisation of pleural inflammation occurring after primary spontaneous pneumothorax, Eur. Respir. J. 23 (6) (2004) 896–900.
[38] M. Noppen, M.H. Baumann, Pathogenesis and treatment of primary spontaneous pneumothorax: an overview, Respiration 70 (4) (2003) 431–438.
[39] M. Noppen, et al., Fluorescein-enhanced autofluorescence thoracoscopy in primary spontaneous pneumothorax, Am. J. Respir. Crit. Care Med. 170 (6) (2004) 680–682.
[40] T. Muramatsu, et al., Cause and management of recurrent primary spontaneous pneumothorax after thoracoscopic stapler blebectomy, Asian J. Surg. 34 (2) (2011) 69–73.
[41] C.H. Park, et al., Risk of primary spontaneous pneumothorax according to chest configuration, Thorac. Cardiovasc. Surg. 66 (7) (2018) 583–588.
[42] C. Karpman, G.L. Aughenbaugh, J.H. Ryu, Pneumothorax and bullae in Marfan syndrome, Respiration 82 (3) (2011) 219–224.
[43] J.R. Hall, et al., Pneumothorax in the Marfan syndrome: prevalence and therapy, Ann. Thorac. Surg. 37 (6) (1984) 500–504.
[44] J.B. West, Distribution of mechanical stress in the lung, a possible factor in localisation of pulmonary disease, Lancet 1 (7704) (1971) 839–841.
[45] S. Nakazawa, et al., Pneumothorax in long-term ventilator users with neuromuscular or neurodegenerative disease, Chest 160 (3) (2021) e323–e324.
[46] W. Yang, et al., Fixation of lung apex in spontaneous pneumothorax is safe and efficient in decrease recurrences, Pediatr Neonatol 60 (1) (2019) 83–86.
[47] L.D.J. Bos, L.B. Ware, Acute respiratory distress syndrome: causes, pathophysiology, and phenotypes, Lancet 400 (10358) (2022) 1145–1156.
[48] J.H. Kim, J.P. Butler, S.H. Loring, Probing softness of the parietal pleural surface at the micron scale, J. Biomech. 44 (14) (2011) 2558–2564.
[49] Y. Akkas, et al., A novel structural risk index for primary spontaneous pneumothorax: ankara Numune Risk Index, Asian J. Surg. 40 (4) (2017) 249–253.